



1 **Development of a dynamic dust-source map for NMME-DREAM v1.0 model based on MODIS**  
2 **NDVI over the Arabian Peninsula**

3 Solomos Stavros<sup>1,2</sup>, Abdelgadir Abuelgasim<sup>2</sup>, Christos Spyrou<sup>3</sup>, Ioannis Biniotoglou<sup>4</sup>, Slobodan  
4 Nickovic<sup>5</sup>

5 **Abstract** We developed a time dependent dust source map for NMME-DREAM v1.0 model  
6 based on the satellite MODIS Normalized Digital Vegetation Index (NDVI). Areas with NDVI<0.1  
7 are classified as active dust sources. The new modeling system is tested for the analysis of dust  
8 particles dispersion over SW Asia using a mesoscale model grid increment of 0.1°×0.1° km for a  
9 period of 1 year (2016). Our results indicate significant deviations in simulated Aerosol Optical  
10 Depths compared to the static dust-source approach and general increase in dustloads over the  
11 selected domain. Comparison with MODIS Aerosol Optical Depth (AOD) indicates a more  
12 realistic spatial distribution of dust in the dynamic source simulations compared to the static  
13 dust sources approach. The modeled AOD bias is improved from -0.140 to 0.083 for the case of  
14 dust events (i.e. for AOD >0.25) and from -0.933 to -0.424 for dust episodes with AOD>1. This  
15 new development can be easily applied to other time periods, models and different areas  
16 worldwide for a local fine tuning of the parameterization and assessment of its performance.

17 <sup>1</sup>Institute for Astronomy, Astrophysics, Space Applications and Remote Sensing (IAASARS), National Observatory of Athens,  
18 Athens, Greece, stavros@noa.gr

19 <sup>2</sup>Department of Geography and Urban Planning, National Space Science and Technology Center, United Arab Emirates  
20 University

21 <sup>3</sup>Department of Geography, Harokopio University of Athens (HUA), El. Venizelou Str. 70, 17671 Athens, Greece.

22 <sup>4</sup>National Institute of R & D for Optoelectronics, Magurele, Ilfov, Romania

23 <sup>5</sup>Republic Hydrometeorological Service of Serbia, Belgrade, Serbia

24 **Keywords:** dust, Arabian Peninsula, DREAM, NDVI, model, satellite

25 **Introduction**

26 The importance of natural particles, namely desert dust, in the weather and climate has  
27 been underlined in a great number of studies. Dust is a climatic regulator, as it modifies  
28 extensively the radiative balance of the atmospheric column (Torge et al., 2011; Spyrou et al.,  
29 2013; Mahowald et al., 2014). At the same time dust aerosols modify the atmospheric water  
30 content (Spyrou 2018), the way clouds are formed by acting as cloud condensation nuclei  
31 (CCN) and ice nuclei (IN) and the precipitation processes (Kumar et al., 2011; Solomos et al.,  
32 2011; Nickovic et al., 2016). In addition, there is a clear connection between dust particles and  
33 human health disorders, as the size of the produced aerosols is small enough to cause  
34 respiratory and cardiovascular diseases, as well as pathogenic conditions due to the  
35 microorganisms that they can potentially carry (Mitsakou et al., 2008; Esmaeil et al., 2014).

36 The Arabian Peninsula is one of the most important sources of mineral dust worldwide and  
37 contributes together with the Saharan and Gobi Deserts in the formation of a North  
38 Hemisphere “dust belt” as described by Prospero et al. (2002). Severe dust storms over the  
39 Peninsula are quite common, especially during long periods without rain, in the spring and



40 summer (Almazrouia et al., 2012). Particles injected into the atmosphere from arid soils, under  
41 favorable weather conditions (high wind speeds and dry soil), can affect large areas around the  
42 sources but also remote locations like the Eastern Mediterranean (Mamouri et al., 2016;  
43 Solomos et al., 2017) and the Indian Ocean (Chakraborty et al. 2006).

44 Due to the multitude and severity of the feedbacks of dust particles not only on the weather  
45 and the ecosystem but to human health as well, the proper description of the production,  
46 transport and eventual deposition of the dust cycle, in numerical weather prediction models  
47 (NWP) is essential. In order to be able to accurately describe the dust life-cycle in the  
48 atmosphere, we need a clear understanding of the areas which can potentially act as “dust  
49 sources”. The definition of such areas dictates the emission strength and therefore the amount  
50 of particles inserted into the atmosphere. A proper representation of dust sources is therefore  
51 an essential first step, in studying the impacts of mineral particles in the climate and human  
52 societies. Usually the definition of the areas that can act as dust sources is made using global  
53 datasets. For example Nickovic et al. (2001) used a subjective correspondence between the  
54 Olson World Ecosystems (Olson et al., 1983) and the thirteen SSiB vegetation types to identify  
55 arid and semi-arid areas. Similarly, Spyrou et al., (2010) used a 30sec global land use/cover  
56 database, classified according to the 24 category U.S. Geological Survey (USGS) land use/cover  
57 system (Anderson et al., 1976), to define active areas in SKIRON dust model. Solomos et al.,  
58 2011 used the LEAF soil and vegetation sub-model of the Regional Atmospheric Modeling  
59 System (RAMS) (Walko et al., 2000) to identify the active dust sources in RAMS-ICLAMS model.

60 However, the above mentioned methodologies have some significant drawbacks. The  
61 datasets are usually not up-to-date, therefore recent land-use modifications are not included  
62 and not represented. In addition, such “static” databases mean that possible seasonal  
63 variations are not taken into account. Towards the direction of overcoming the above  
64 limitations and improving global dust forecasts, Kim et al., 2013 developed a dynamical dust  
65 source map for the GOCART dust model by characterizing NDVI values  $< 0.15$  as active dust  
66 spots. Similarly Vukovic et al., 2014 combined MODIS landcover types with pixels having NDVI  $<$   
67  $0.1$  to identify the seasonal dust sources that enforced the severe Phoenix haboob of July 2011  
68 in the US. Such information can be even more relevant at meso and local scales for determining  
69 landuse changes and potential dust sources, especially in heterogeneous regions such as the  
70 Arabian Peninsula and the greater SW Asia. In this context, Solomos et al., 2017, used the  
71 Landsat-8 NDVI data (assuming also NDVI  $< 0.1$  as active sources) to identify recent changes in  
72 landuse due to the war in Iraq and Syria resulting in a significantly more realistic simulation of  
73 dust properties in the Middle East.

74 In the current study we present the implementation of a dynamical dust source map in the  
75 well-established and widely used DREAM v1.0 dust model (Nickovic et al., 2001; Perez et al.,  
76 2006). The new development is first tested here for the greater SW Asia but can be extended  
77 for use in mesoscale dust modeling applications worldwide. Two experimental simulations are  
78 performed for one month period (August 2016) over the greater SW Asia: 1) Control run, where  
79 the dust source definition is based on Olson World Ecosystems dataset and 2) Dynamic source  
80 run, where the NDVI values are used to identify the dust sources. The model results from both  
81 runs are compared to available satellite observations and station measurements inside the  
82 modeling domain. In section 1 we describe the methodological steps regarding the model



83 developments and remote sensing data; Section 2 includes the results of the experimental runs  
84 and section 3 is a summary and discussion of the study findings.

85

86

## 87 1. Methodology

88

### 89 1.1. Model description

90 The modeling system used in this study is NMME-DREAM v1.0. The meteorological core is  
91 the NCEP/NMME atmospheric model (Janjic et al., 2001). The Dust Regional Atmospheric Model  
92 (DREAM v1.0) is a numerical model created with the main purpose to simulate and predict the  
93 atmospheric life-cycle of mineral dust using an Euler-type partial differential nonlinear equation  
94 for dust mass continuity (Nickovic et al., 2001; Perez et al., 2006; Pejanovic et al., 2011, Nickovic  
95 et al., 2016). Once particles have been lifted from the ground they are driven by the  
96 atmospheric model variables and processes. Therefore turbulent parameters are used in the  
97 beginning of the process, when dust is lifted from the ground, and transported by model winds  
98 in the later phases when dust travels away from the sources. Dust is eventually settled through  
99 rainfall and/or dry deposition processes.

100 In order to test the use of NDVI for source characterization, the model is setup with a  
101 horizontal resolution of  $0.1^\circ \times 0.1^\circ$ , covering the Arabian Peninsula parts of SW Asia and parts of  
102 NE Africa (Figure 1). On the vertical we use 28 levels stretching from the surface to the top of  
103 the atmosphere. August 2016 has been selected as a test period for the model development  
104 due to the significant dust activity and variability in wind properties during this month. The  
105 original classification of dust sources in DREAM is based on Ginoux et al., 2001 that takes into  
106 account the preferential sources related to topographic depressions and paleolake sediments.  
107 In our work, a numerical procedure has been developed to insert the NDVI satellite information  
108 into the model and to update such info each time the NDVI changes, during the simulation  
109 period. We assume that regions with NDVI values from 0 to 0.1 correspond to bare soil and  
110 therefore can be efficient sources (“dust points”; DeFries and Townshend, 1994; Solomos et al.,  
111 2017). The NDVI dataset is at finer resolution than the model grid and in order to find the  
112 potential for dust production in each model grid box, we calculate the following ratio:

$$A_{grid\_box} = \frac{\#\_of\_dust\_point\ s}{Total\_#\_of\_point\ s}$$

113

114

115

116

117

118

119

120

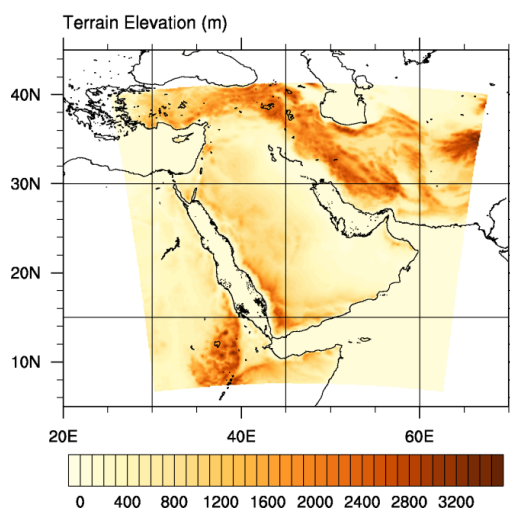
121

122

This approach allows for a dynamic description of dust source areas over the model domain to  
replace the previously used static database. Moreover, the scaling of satellite data over model  
grid points allows the use of the same algorithm for different model configurations.  
Additionally, we have applied a limit to dust efficiency over high mountains. Several mountains  
in the area (e.g. the Sarawat Mountains along the Red Sea coast and the Zagros Mountains in  
Iraq) could be misclassified as dust sources due to low NDVI values. These areas need to be  
excluded from the new dust-source map and the modeled dust efficiency is modified  
accordingly.



122 In Figure 2a we show the static sources in the original model version with a factor of 0 to 1  
 123 depending on the source area strength. Accordingly in Figure 2b we show the new dynamic  
 124 sources for August 2016.



125

126

**Figure 1: DREAM model domain and topography in meters**

127 **1.2 NDVI description**

128 For the purposes of our study we used the 500m 16-day averaged NDVI from MODIS (Didan,  
 129 2015) for the period of interest. The NDVI is a normalized transform of the near infrared to red  
 130 reflectance ratio, designed to provide a standard for vegetation and takes values between -1  
 131 and +1. Since it is expressed as a ratio, the NDVI has the advantage of minimizing certain types  
 132 of band-correlated noise (positively-correlated) and influences attributed to variations in  
 133 irradiance, clouds, atmospheric attenuation and other parameters (Solano et al., 2010).

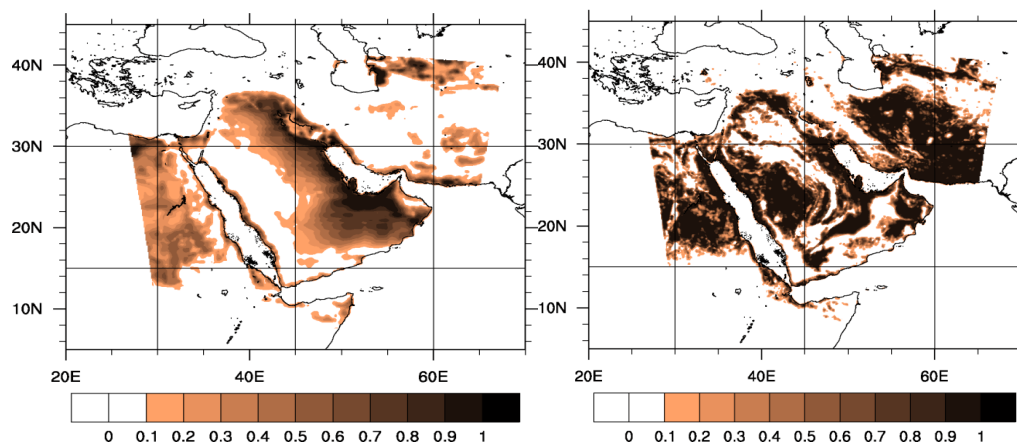
134 To create an accurate time-dependent dust source map, we have utilized the Normalized  
 135 Difference Vegetation Index (NDVI) derived from the MODIS/Terra instrument. NDVI is  
 136 calculated as the normalized difference of reflectance in the red and near-infrared channels  
 137 (Rouse et al., 1974; Huete et al. 2002) i.e.,

$$NDVI = \frac{X_{nir} - X_{red}}{X_{nir} + X_{red}}$$

138 where X represents the top of the atmosphere reflectance in each channel. For terrestrial  
 139 targets, NDVI will take values near 0.8 for vegetated areas and near 0 for barren soil (Huete et  
 140 al., 1999). Since it is expressed as a ratio, the NDVI has the advantage of minimizing certain  
 141 types of noise and influences attributed to variations in irradiance, clouds, cloud-shadows,  
 142 atmospheric attenuation, and other parameters (Solano et al., 2010). Specifically, we have used  
 143 the 500m 16-day averaged NDVI from MODIS/Terra instrument (Didan, 2015) to calculate high-  
 144 resolution barren soil. The high-resolution masks was used to calculate the percentage of  
 145 barren land in each 0.1°x0.1° model grid cells and this percentage was used to define the  
 146 effective strength of dust sources in each cell.



147



148

149

150

151 **Figure 2: Dust source strength as defined by (a) the Ginoux et al., 2001 dataset and (b) the**  
152 **August 2016 NDVI**

153

154 **2. Results**

155 In order to test the performance of the new methodology we run the model in two different  
156 configurations: (1) Using the static Ginoux et al., 2001 dust source database, called CTRL\_run  
157 from now on, and (2) using the dynamic NDVI database as described above, called NDVI\_run  
158 from now on. Both setups are initialized using the NCEP GFS analysis files (0.5°×0.5° at 00, 06,  
159 12 and 18 UTC), which were used for boundary conditions as well. The two model  
160 configurations are identical other than the dust source database. The test simulation period is  
161 1-31 August 2016 and the results from both simulations are compared to MODIS and AERONET  
162 AOD until we conclude to an optimal model setup. A five days spin up model run, prior to the  
163 experimental period, is used for establishing the dust background over the domain. After  
164 finalizing the experimental model configuration we perform a complete one-year run (2016)  
165 and evaluate the results against AERONET stations.

166 **2.1 Dust transport during August 2016**

167 The selected 1-month period is characterized by a significant variability in wind speeds and  
168 directions which allows the evaluation of the new model version under different conditions.  
169 During 1-10 August, east winds prevail over the region and increased dust concentrations are  
170 found mostly along the central, east and south coastal areas of the Arabian Peninsula. An  
171 anticyclonic circulation is established during 10-15 over the Arabia Desert and increased dust  
172 concentrations are mostly found over the central desert areas. On 16-26 August the circulation  
173 is mainly from north directions and thick dust plumes are advected southwards towards the  
174 Arabian Sea. The north winds veer to east on 26-31 August and increased dustloads are found  
175 over the Arabian Gulf during these dates.



176

177 **2.2 Comparison with MODIS and AERONET**

178 The monthly average AOD for August 2016 is shown in Figure 3 for the two experimental runs  
179 (Figure 3a,b). The NDVI\_run results in a significantly modified spatial distribution of dust  
180 presenting increased dustloads over the entire domain and most profoundly over the Red Sea  
181 and Arabian Gulf (Figure 3b). This dust pattern is closer to the MODIS observed AOD over the  
182 same period that is shown in Figure 3c. The MODIS AOD in this area is mostly related to dust,  
183 however it must be taken into account that other aerosols not parameterized in the model (e.g.  
184 sea salt, sulphates, nitrates) may also contribute to the observed MODIS AOD.

185 More specifically the NDVI\_run reproduces the MODIS observed AOD pattern that is in general  
186 characterized by values 0.3-0.4 at the NW parts of the Arabian Peninsula and by values 0.4-0.8  
187 at the SE parts. Significant improvement is also evident over the Red Sea and NE Africa. The  
188 NDVI\_run captures the maximum observed AOD values reaching up to 1.6 over the Red Sea and  
189 also the southwesterly extension of an AOD tongue of 0.3-0.8 towards Soudan. At the east  
190 parts of the modeling domain the NDVI\_run again outperforms the CTRL\_run since it  
191 reproduces the spatial distribution of AOD 0.4-0.8 over the Arabian Sea and the maximum of  
192 0.8-1.2 at the SE edge of Arabian Peninsula. Inside the Gulf, the NDVI run correctly represents  
193 the 0.4-0.8 AOD but the dust concentration is over-predicted at the Strait of Hormuz and along  
194 the Iran - Pakistan coastline. This is mostly due to the prevailing NE winds during the last days of  
195 the August 2016 modeling period and due to a possible miss-classification of Iran and Pakistan  
196 grid points as effective dust sources thus favoring unrealistic southeasterly transport towards  
197 the Gulf of Oman.

198 As a second step we run the same model configurations (CTRL and NDVI) for the entire 2016.  
199 The modeled dust optical depth is compared with the regional AERONET ground-based  
200 photometric measurements of AOD considering only dust relevant measurements with  
201 Angström Coefficient <0.6 (Holben et al., 1998) and the results are shown in Table 1. For  
202 completeness we first consider all AERONET stations inside the modeling domain for the  
203 evaluation. However the stations that are at the margins of our domain (Cairo\_EMA\_2,  
204 SEDE\_BOKER, AgiaMarina\_Xyliatou and El\_Farafra) are also affected by other dust source areas  
205 (e.g. Sahara Desert) and their statistics are not representative for Arabian and Middle East  
206 sources. Instead, the comparison with Arabian Peninsula stations (Eilat, Kuwait\_University,  
207 KAUST\_Campus and Mezaira) provides more insight on the effects of the new source  
208 characterization. As seen in Figure 4 and also in Table2 these stations are clearly benefited from  
209 the experimental run.

210 In general the two runs present a significant statistical difference and more remarkably a  
211 reverse of bias (MODEL-AERONET) from negative in the CTRL\_run to positive in the NDVI\_run.  
212 The NDVI\_run produces increased AODs that are neither linearly proportional to the CTRL\_run  
213 AODs nor uniformly distributed over the domain. When considering only Arabian stations, the  
214 statistical metrics in Table 1 and especially the fractional gross error and bias are improved but  
215 the RMSE is increased due to the increase in maximum modeled AODs. In order to investigate



216 the sensitivity of our results towards the severity of dust events we further assume two  
 217 additional air quality states in Table 1: (i) dust events (AOD>0.25) and (ii) severe dust episodes  
 218 (AOD>1). The bias reverse is evident in both cases however when considering AOD>1 even the  
 219 NDVI run under-predicts the dustloads however with a lower RMSE (0.586 versus 0.983). This is  
 220 clearly evident in Figure 5 where the NDVI run is indeed more realistic but still does not  
 221 reproduce the extreme AOD during severe episodes. For most of the cases such high AODs  
 222 should be attributed to duststorms from convective downdrafts (haboobs). These processes are  
 223 not resolved at mesoscale model resolutions (Solomos et al., 2012, 2017; Vukovic et al., 2014)  
 224 and thus cannot be represented here.

225 **Table 1. Statistical metrics from the comparison between model runs and AERONET photometers**

	Mean bias (Model-Observation)		RMSE		Correlation		Fractional gross error		Mean fractional bias	
	CTRL	NDVI	CTRL	NDVI	CTRL	NDVI	CTRL	NDVI	CTRL	NDVI
AOD > 0 (All Stations)	-0.163	0.015	0.258	0.312	0.408	0.464	0.887	0.803	-0.639	0.043
AOD > 0 (Arabia Stations)	-0.142	0.122	0.252	0.332	0.340	0.426	0.644	0.515	-0.455	-0.187
AOD > 0.25 (Arabia Stations)	-0.140	0.083	0.283	0.350	0.238	0.328	0.640	0.462	-0.527	-0.142
AOD > 1 (Arabia Stations)	-0.933	-0.424	0.983	0.586	0.032	0.009	1.230	0.481	-1.211	-0.413

The AERONET stations used in this study are: Eilat (29N,34E), Cairo\_EMA\_2 (30N,31E), Kuwait\_University (29N,47E), KAUST\_Campus (22N,39E), SEDE\_BOKER (30N,34E), AgiaMarina\_Xyliatou (35N,33E), Mezaira (23N,53E) and El\_Farafra (27N,27E)

226 **3. Summary and Discussion**

227 Previous attempts to scale the dust emissions by satellite NDVI in the global model GOCART  
 228 (Kim et al., 2013), the mesoscale model NMME-DREAM v1.0 (Vukovic et al., 2014) and in the  
 229 high resolution model RAMS-ICLAMS (Solomos et al., 2017) showed the potential of this  
 230 approach for replacing the static dust source maps in the models by a dynamic dataset. In this  
 231 study we present the development of a dynamic dust source map for implementation in  
 232 NMME-DREAM v1.0 over the Arabian Peninsula and the greater areas of Middle East, SW Asia  
 233 and NE Africa. Although the major dust sources worldwide are located in permanent deserts  
 234 where the NDVI is almost always <0.1 (e.g. Bodele Depression, Gobi Desert, Arabian Desert),  
 235 the dynamical scaling of dust emissions presented here can be important for providing up-to-  
 236 date evidence of active dust sources over non-permanent deserts. These may include bog,  
 237 marsh and semi-desert areas as well as irrigated and non-irrigated farms where landuse  
 238 changes occur throughout the year. Analysis of the modeling results for one year test period  
 239 (2016) over SW Asia indicated the improved performance of the new parameterization. The  
 240 NDVI\_run showed a significant increase in dustloads over the greater Arabian Peninsula area  
 241 and a more realistic representation of the spatial distribution of AOD compared to the



242 corresponding MODIS satellite retrievals. Comparison with AERONET measurements also  
 243 showed significant improvement especially at higher AODs that are also relevant to the model  
 244 efficiency for air quality purposes (i.e. the model bias is reduced from -0.140 to 0.083 at  
 245 AOD>0.25 and from -0.933 to -0.424 at AOD>1). However, the model statistics are not  
 246 improved for all AERONET measuring stations and for all air quality states (Table2), mainly due  
 247 to a possible misclassification of dust sources in the highlands of Iran and Pakistan.

248 The main purpose of our work was the development and first testing of this new modeling  
 249 version. A major advance of our study is the ability to implement the real-time properties of  
 250 dust sources in air quality simulations (as represented by the satellite NDVI) and thus capture  
 251 local or seasonal effects. In general, one year is not sufficient for extracting robust statistical  
 252 results and further analysis is required to examine the performance of the proposed  
 253 methodology over longer time periods and also over different areas worldwide. For example  
 254 the simple approach of employing a uniform value of NDVI<0.1 for determining the active dust  
 255 sources may not be adequate to represent fine-scale land properties and further adjustments  
 256 may be required depending on local-scale characteristics. This new approach for the dynamic  
 257 characterization of active dust sources based on NDVI can be easily implemented in other  
 258 atmospheric dust models at different configurations and spatial coverage for improving their  
 259 performance.

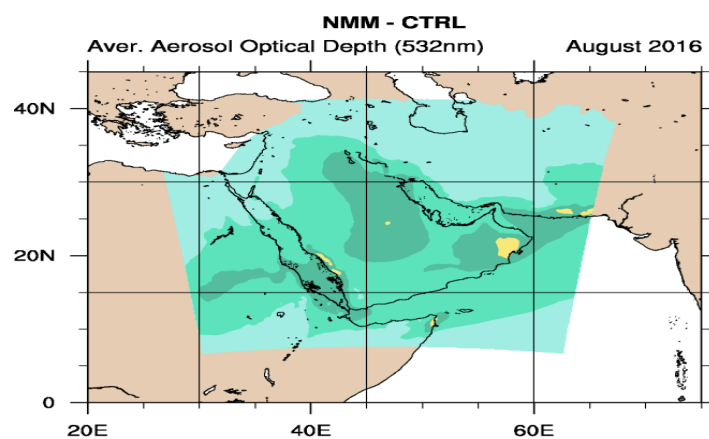
260 **Table 2. Statistical metrics at AERONET stations**

Station	Mean bias		RMSE		Correlation		Fractional gross error		Mean fractional bias	
	CTRL	NDVI	CTRL	NDVI	CTRL	NDVI	CTRL	NDVI	CTRL	NDVI
AgiaMarina_Xyliatou	-0.188	-0.185	0.226	0.224	-0.005	0.001	1.825	1.780	-1.828	-1.767
Cairo_EMA_2	-0.355	-0.344	0.406	0.399	-0.053	0.018	1.689	1.646	-1.687	-1.591
Eilat	-0.138	0.006	0.186	0.165	0.110	0.312	1.183	0.610	-1.166	0.034
El_Farafra	-0.186	-0.190	0.259	0.263	0.170	0.138	1.155	1.248	-1.218	-1.257
KAUST_Campus	-0.245	0.152	0.322	0.376	0.412	0.386	0.966	0.609	-1.001	0.342
Kuwait_University	-0.097	0.007	0.275	0.278	0.152	0.266	0.588	0.537	-0.290	0.018
Mezaira	-0.130	0.161	0.228	0.347	0.353	0.445	0.528	0.475	-0.382	0.332
SEDE_BOKER	-0.151	-0.125	0.198	0.201	0.030	0.034	1.202	1.209	-1.228	-0.921
Weizmann_Institute	-0.207	-0.180	0.264	0.255	-0.088	-0.100	1.494	1.323	-1.521	-1.197

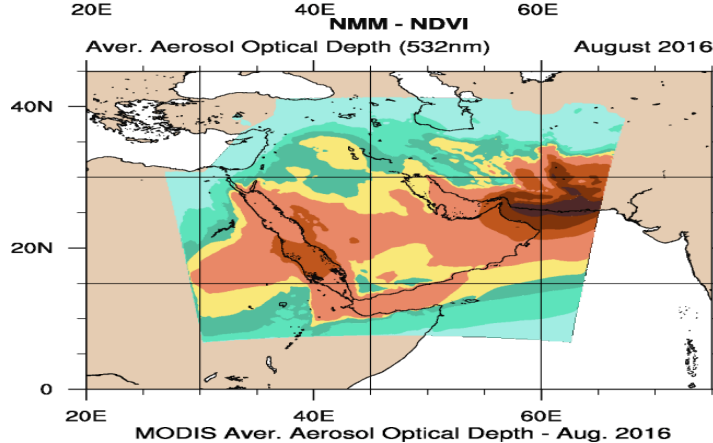
261



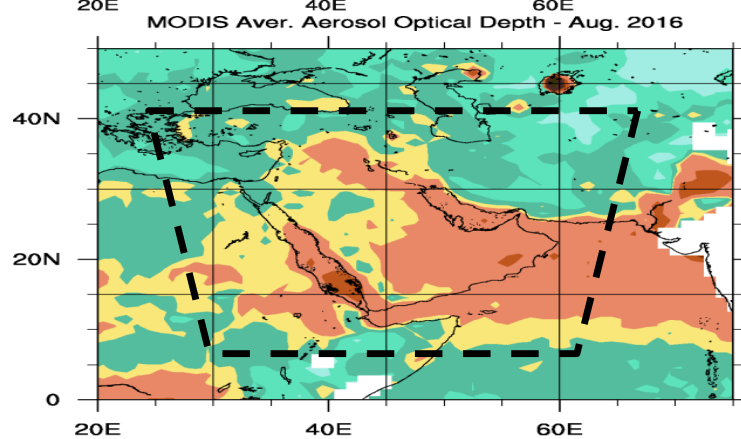
262



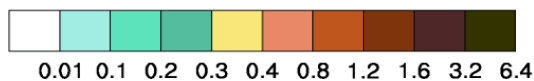
263



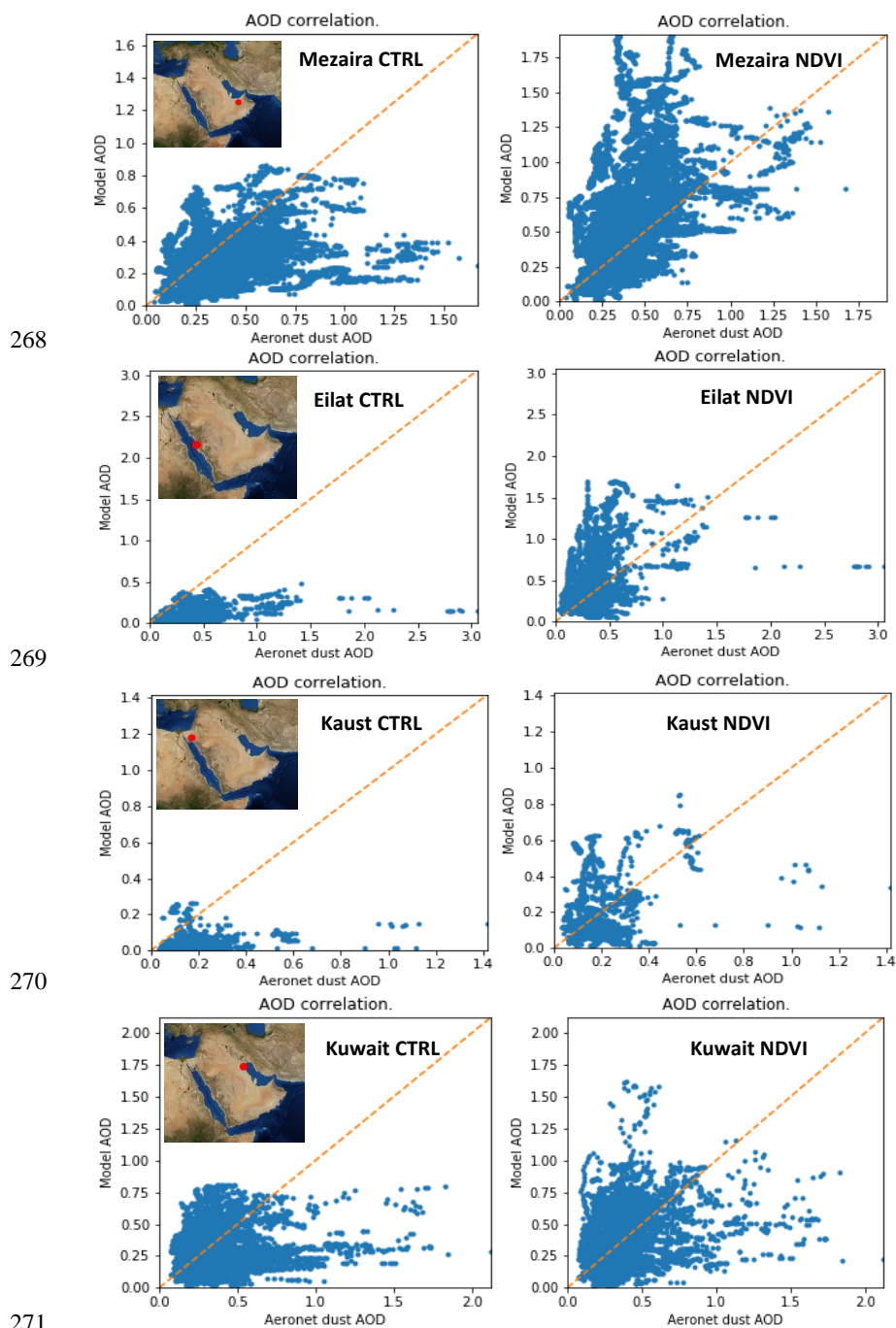
264



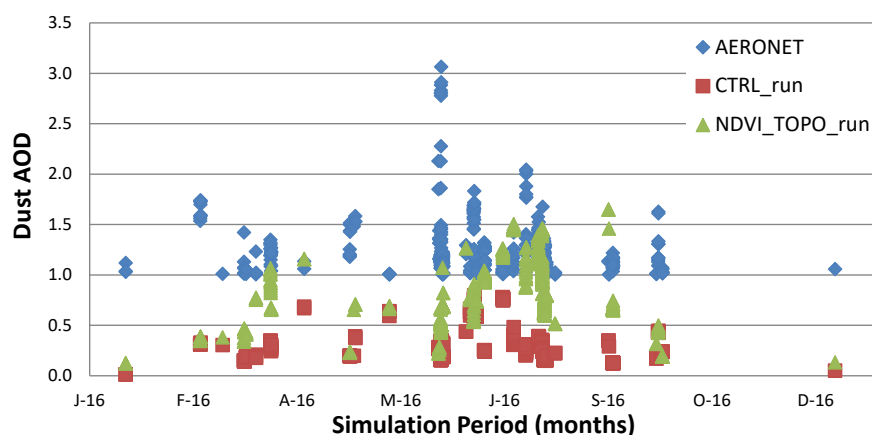
265



266 Figure 3. Monthly average simulated AOD during August 2016 from CTRL\_run (a), NDVI\_run (b)  
267 and (c) MODIS. The dashed trapezoid in (c) denotes the location of the modeling domain.



272 Figure 4. Correlation plots of modeled and AERONET dust AOD at the stations of Mezaira, Eilat,  
273 Kaust and Kuwait for 2016.



274

275 Figure 5. Timeseries of measured and modeled dust AOD for the cases of AERONET AOD>1

276

### 277 Code and Data availability

278 All code and data used in this study are available upon request

### 279 Author Contribution

280 SS: Conceptualization, Formal analysis, Investigation, Methodology, Project administration,  
281 Resources, Software, Validation, Visualization, Writing - original draft, Writing - review &  
282 editing;

283 AA: Conceptualization, Funding acquisition, Project administration, Supervision, Writing -  
284 review & editing;

285 CS: Software, Data curation, Visualization, Writing - review & editing;

286 IB: Conceptualization, Formal analysis, Software, Writing - review & editing;

287 SN: Methodology, Supervision, Writing - review & editing;

### 288 Acknowledgements

289 This work was funded by a grant from the National Space Science and Technology Center of the  
290 United Arab Emirates University under grant number NSS Center 7 -2017.

291



## 292 References

- 293 Almazrouia, M., M. Nazrullslama, P.D. Jonesa, H. Athara and M. AshfaqurRahmana, Recent  
294 climate change in the Arabian Peninsula: Seasonal rainfall and temperature climatology of Saudi  
295 Arabia for 1979–2009. *Atmospheric Research*, 111, July 2012, p.p. 29–45., 2012
- 296 Anderson, J., E. Hardy, J. Roach, and R. Witmer, A land use and land cover classification  
297 system for use with remote sensing data, U.S. Geol. Prof. Pap. 964, U.S. Gov. Print.Off.,  
298 Washington, D. C., 1976
- 299 ChakrabortyArindam, Ravi S. Nanjundiah and J. Srinivasan, Impact of African orography and  
300 the Indian summer monsoon on the low-level Somali jet, *Int. J. Climatol.* 29: 983–992 (2009),  
301 DOI: 10.1002/joc.1720, 2009
- 302 DeFries, R. S. and Townshend, J. R. G.: NDVI-derived land cover classifications at a global  
303 scale, *Int. J. Remote Sens.*, 15, 3567–3586, doi:10.1080/01431169408954345, 1994.
- 304 Didan, K. , MOD13A1 MODIS/Terra Vegetation Indices 16-Day L3 Global 500m SIN Grid V006  
305 [Data set]. NASA EOSDIS LP DAAC. doi: 10.5067/MODIS/MOD13A1.006, 2015
- 306 Esmaeil N., M. Gharagozloo, A. Rezaei, G. Grunig, 2014. Dust events, pulmonary diseases and  
307 immune system, *Am J ClinExplmmunol* 2014 3(1):20-29, 2014.
- 308 Ginoux, P., Chin, M., Tegen, I., Prospero, J. M., Holben, B., Dubovik, O., & Lin, S.-J., Sources  
309 and distributions of dust aerosols simulated with the GOCART model. *Journal of Geophysical*  
310 *Research*, 106(D17), 20,255–20,273. <https://doi.org/10.1029/2000JD000053>, 2001
- 311 Holben, B.N., Eck, T.F., Slutsker, I., Tanre, D., Buis, J.P., Setzer, A., Vermote, E., Reagan, J.A.,  
312 Kaufman, Y., Nakajima, T., Lavenu, F., Jankowiak, I., Smirnov, A., AERONET a federated  
313 instrument network and data archive for aerosol characterization. *Rem. Sens. Environ.* 66,  
314 1e16., 1998
- 315 Huete, A. R., Justice, C., and van Leeuwen, W., MODIS Vegetation index (MOD 13): Algorithm  
316 Theoretical Basis Document, NASA Goddard Space Flight Center, Greenbelt, Maryland 20771,  
317 1999
- 318 Huete, A., Didan, K., Miura, T., Rodriguez, E. P., Gao, X., & Ferreira, L. G., Overview of the  
319 radiometric and biophysical performance of the MODIS vegetation indices. *Remote Sensing of*  
320 *Environment*, 83, 195–213., 2002
- 321 Janjic, Z.I., Gerrity J.P.Jr., and *Nickovic, S.*, An Alternative Approach to Nonhydrostatic  
322 Modeling. *Monthly Weather Review*, 129: 1164-1178., 2001
- 323 Kim, D., M. Chin, H. Bian, Q. Tan, M. E. Brown, T. Zheng, R. You, T. Diehl, P. Ginoux, and T.  
324 Kucsera, The effect of the dynamic surface bareness on dust source function, emission, and  
325 distribution, *J. Geophys. Res. Atmos.*, 118, 871–886, doi: 10.1029/2012JD017907., 2013
- 326 Kumar, P., Sokolik, I. N., and Nenes, A.: Measurements of cloud condensation nuclei activity  
327 and droplet activation kinetics of fresh unprocessed regional dust samples and minerals,  
328 *Atmos. Chem. Phys.*, 11, 3527–3541, doi:10.5194/acp-11-3527-2011, 2011.
- 329 Mahowald, N, Albani, S., Kok, J. F., Engelstaeder, S., Scanza, R., Ward, D.S., Flanner, M.G.,  
330 The size distribution of desert dust aerosols and its impact on the Earth system, *Aeolian*  
331 *Research*, 15, 2014, Pages 53-71, <https://doi.org/10.1016/j.aeolia.2013.09.002>., 2014
- 348 Mamouri, R.-E., Ansmann, A., Nisantzi, A., Solomos, S., Kallos, G., and Hadjimitsis, D. G.:  
349 Extreme dust storm over the eastern Mediterranean in September 2015: satellite, lidar, and



- 350 surface observations in the Cyprus region, *Atmos. Chem. Phys.*, 16, 13711-13724,  
351 <https://doi.org/10.5194/acp-16-13711-2016>, 2016
- 352 Mitsakou, C., Kallos, G., Papantoniou, N., Spyrou, C., Solomos, S., Astitha, M., and Housiadis,  
353 C.: Saharan dust levels in Greece and received inhalation doses, *Atmos. Chem. Phys.*, 8, 7181-  
354 7192, <https://doi.org/10.5194/acp-8-7181-2008>, 2008.
- 355 Nickovic, S., G. Kallos, A. Papadopoulos, and O. Kakaliagou, A model for prediction of desert  
356 dust cycle in the atmosphere, *J. Geophys. Res.*, 106(D16), 18,113–18,129, 2001
- 357 Nickovic, S., Cvetkovic, B., Madonna, F., Rosoldi, M., Pejanovic, G., Petkovic, S., and Nikolic,  
358 J.: Cloud ice caused by atmospheric mineral dust – Part 1: Parameterization of ice nuclei  
359 concentration in the NMME-DREAM model, *Atmos. Chem. Phys.*, 16, 11367-11378,  
360 <https://doi.org/10.5194/acp-16-11367-2016>, 2016.
- 361 Olson, J. S., J. A. Watts and L. J. Allison, Carbon in Live Vegetation of Major World  
362 Ecosystems, Report ORNL-5862, Oak Ridge National Laboratory, Oak Ridge, Tennessee, USA.,  
363 1983
- 364 Pejanovic, G., S. Nickovic, M. Vujadinovic, A. Vukovic, V. Djurdjevic, M. Dacic, Atmospheric  
365 deposition of minerals in dust over the open ocean and possible consequences on climate.  
366 WCRP OSC Climate Research in Service to Society, 24-28 October 2011, Denver, CO, USA, 2011
- 367 Pérez, C., S. Nickovic, J. M. Baldasano, M. Sicard, F. Rocadenbosch, and V. E. Cachorro, A long  
368 Saharan dust event over the western Mediterranean: Lidar, Sun photometer observations, and  
369 regional dust modeling, *J. Geophys. Res.*, 111, D15214, doi:10.1029/2005JD006579., 2006
- 370 Prospero J. M., P. Ginoux, O. Torres, S. E. Nicholson, and T. E. Gill, Environmental  
371 characterization of global sources of atmospheric soil dust identified with the nimbus 7 total  
372 ozone mapping spectrometer (TOMS) absorbing aerosol product, *Rev. Geophys.*, 40(1), 1002,  
373 doi:10.1029/2000RG000095, 2002
- 374 Rouse Jr, R. H. Haas, J. A. Schell, and D. W. Deering. "Monitoring vegetation systems in the  
375 Great Plains with ERTS."In NASA. Goddard Space Flight Center 3d ERTS-1 Symp., Vol. 1, Sect. A p  
376 309-317, 1974
- 377 Solano, R., K., Didan , A., Jacobson and A. Huete, MODIS Vegetation Index User's Guide, ver.  
378 2.0, Vegetation Index and Phenology Lab, <http://vip.arizona.edu>, The University of Arizona.,  
379 2010
- 380 Solomos, S., Kallos, G., Kushta, J., Astitha, M., Tremback, C., Nenes, A., and Levin, Z.: An  
381 integrated modeling study on the effects of mineral dust and sea salt particles on clouds and  
382 precipitation, *Atmos. Chem. Phys.*, 11, 873–892, doi:10.5194/acp-11-873-2011, 2011.
- 383 Solomos, S., Ansmann, A., Mamouri, R.-E., Biniotoglou, I., Patlakas, P., Marinou, E., and  
384 Amiridis, V.: Remote sensing and modelling analysis of the extreme dust storm hitting the  
385 Middle East and eastern Mediterranean in September 2015, *Atmos. Chem. Phys.*, 17, 4063-  
386 4079, <https://doi.org/10.5194/acp-17-4063-2017>, 2017
- 387 Spyrou, C., Direct radiative impacts of desert dust on atmospheric water content, *Aerosol*  
388 *Science and Technology*, DOI: 10.1080/02786826.2018.1449940., 2018
- 389 Spyrou, C., G. Kallos, C. Mitsakou, P. Athanasiadis, C. Kalogeri and M. J. Iacono, 2013:  
390 Modeling the radiative effects of desert dust on weather and regional climate. *Atmos. Chem.*  
391 *Phys.*, 13, 5489–5504, doi:10.5194/acp-13-5489-2013, 2013



- 392 Spyrou, C., C. Mitsakou, G. Kallos, P. Louka, and G. Vlastou, An improved limited area model  
393 for describing the dust cycle in the atmosphere, *J. Geophys. Res.*, 115, D17211,  
394 doi:10.1029/2009JD013682., 2010
- 395 Torge, A., Macke, A., Heinold, B. And Wauer, J., Solarradiative transfer simulations in  
396 Saharan dust plumes: particle shapes and 3-D effect. *Tellus B*, 63: 770-780. doi:10.1111/j.1600-  
397 0889.2011.00560.x, 2011
- 398 Vukovic, A., Vujadinovic, M., Pejanovic, G., Andric, J., Kumjian, M. R., Djurdjevic, V., Dacic,  
399 M., Prasad, A. K., El-Askary, H. M., Paris, B. C., Petkovic, S., Nickovic, S., and Sprigg, W. A.:  
400 Numerical simulation of "an American haboob", *Atmos. Chem. Phys.*, 14, 3211-3230,  
401 <https://doi.org/10.5194/acp-14-3211-2014>, 2014
- 402 Walko RL, Band LE, Baron J, Kittel TGF, Lammers R, Lee TJ, Ojima D, Pielke RA Sr, Taylor C,  
403 Tague C, Tremback CJ, Vidale PJ, Coupled atmosphere-biophysichydrology models for  
404 environmental modeling. *J Appl Meteor* 39: 931–944, 2000